



# 1 A new smog chamber system for atmospheric multiphase 2 chemistry study: design and characterization

3 Taomou Zong<sup>1</sup>, Zhijun Wu<sup>1,2,\*</sup>, Junrui Wang<sup>1,3</sup>, Kai Bi<sup>4</sup>, Wenxu Fang<sup>1</sup>, Yanrong Yang<sup>1</sup>,  
4 Xuena Yu<sup>1</sup>, Zhier Bao<sup>5</sup>, Xiangxinyue Meng<sup>1</sup>, Yuheng Zhang<sup>1</sup>, Song Guo<sup>1,2</sup>, Yang  
5 Chen<sup>5</sup>, Chunshan Liu<sup>6</sup>, Yue Zhang<sup>7</sup>, Shao-Meng Li<sup>1</sup>, Min Hu<sup>1,2</sup>

6 <sup>1</sup>State Key Joint Laboratory of Environmental Simulation and Pollution Control, College of  
7 Environmental Sciences and Engineering, Peking University, Beijing 100871, China

8 <sup>2</sup>Collaborative Innovation Center of Atmospheric Environment and Equipment Technology, Nanjing  
9 University of Information Science and Technology, Nanjing 210044, China

10 <sup>3</sup>Laboratory of Atmospheric Observation Supersite, School of Environment and Energy, Peking  
11 University Shenzhen Graduate School, Shenzhen 518055, China

12 <sup>4</sup>Beijing Key Laboratory of Cloud, Precipitation and Atmospheric Water Resources, Beijing, 100089,  
13 China

14 <sup>5</sup>Research Center for Atmospheric Environment, Chongqing Institute of Green and Intelligent  
15 Technology, Chinese Academy of Sciences, Chongqing, 400714, China

16 <sup>6</sup>Beijing Convenient Environmental Tech Co. Ltd., Beijing 101115, China

17 <sup>7</sup>Department of Atmospheric Sciences, Texas A&M University, College Station, TX 77843, United States

18 *Correspondence to:* Zhijun Wu ([zhijunwu@pku.edu.cn](mailto:zhijunwu@pku.edu.cn))

## 19 **E-mail lists:**

20 Taomou Zong ([zongtaomou@pku.edu.cn](mailto:zongtaomou@pku.edu.cn))

21 Zhijun Wu ([zhijunwu@pku.edu.cn](mailto:zhijunwu@pku.edu.cn))

22 Junrui Wang ([18845725921@163.com](mailto:18845725921@163.com))

23 Kai Bi ([bikai\\_picard@vip.sina.com](mailto:bikai_picard@vip.sina.com))

24 Wenxu Fang ([343299989@qq.com](mailto:343299989@qq.com))

25 Yanrong Yang ([yxr2020@stu.pku.edu.cn](mailto:yxr2020@stu.pku.edu.cn))

26 Xuena Yu ([99784925@qq.com](mailto:99784925@qq.com))

27 Zhier Bao ([baozhier@cigit.ac.cn](mailto:baozhier@cigit.ac.cn))

28 Xiangxinyue Meng ([mxxxy96@126.com](mailto:mxxxy96@126.com))

29 Yuheng Zhang ([zhangyh@stu.pku.edu.cn](mailto:zhangyh@stu.pku.edu.cn))

30 Song Guo ([guosong@pku.edu.cn](mailto:guosong@pku.edu.cn))

31 Yang Chen ([chenyang@cigit.ac.cn](mailto:chenyang@cigit.ac.cn))

32 Chunshan Liu ([bjkwnt@163.com](mailto:bjkwnt@163.com))

33 Yue Zhang ([Yuezhang@tamu.edu](mailto:Yuezhang@tamu.edu))

34 Shao-Meng Li ([shaomeng.li@pku.edu.cn](mailto:shaomeng.li@pku.edu.cn))

35 Min Hu ([minhu@pku.edu.cn](mailto:minhu@pku.edu.cn))

36

37

38



39 **Abstract.** Multiphase chemistry is an important pathway for the formation of secondary organic aerosols  
40 in the atmosphere. In this study, an indoor 2 m<sup>3</sup> Teflon chamber system (Aerosol multiphase chemistry  
41 Research chamber, AIR) was developed and characterized to specifically simulate atmospheric  
42 multiphase chemistry processes. The temperature and humidity controls, diurnal variation simulation,  
43 and seed particle generation unit in this chamber system were designed to meet the needs of simulating  
44 multiphase atmospheric chemical reactions. The AIR chamber is able to accurately control temperature  
45 (2.5 ~ 31 ± 0.15 °C) and relative humidity (RH < 2 % ~ > 95% ± 0.75%) over a relatively broad range.  
46 In addition, an RH regulation module inside the chamber was designed to simulate the diurnal variation  
47 of ambient atmospheric RH. The aerosol generation unit is able to generate pre-deliquest seed  
48 particles with an organic coating across a wide range of phase states or morphologies. The organic  
49 coating thickness of the aerosols within the chamber can be precisely controlled through adjusting the  
50 condensation temperature, further helping to elucidate the roles of seed particles in multiphase chemical  
51 reactions. The inner walls of the AIR chamber are passivated to reduce the wall loss rates of reactive  
52 gases. Yield experiments of  $\alpha$ -pinene ozonolysis with and without seed particles combined with a box  
53 model simulation demonstrate the high-quality performance of secondary aerosol formation simulation  
54 using the AIR chamber.

## 55 **1 Introduction**

56 Smog chamber is a mainstream tool in chemical laboratory studies to simulate the formation and  
57 evolution of air pollutants (Batchvarova et al., 2006; Chen and Lelevkin, 2006; Kolev and Grigorjeva,  
58 2006; Mocanu et al., 2006; Tolkacheva, 2006) and reveal the parameterization or mechanisms of  
59 atmospheric processes (Wenger, 2006; Olariu et al., 2006; Bejan et al., 2006; Mellouki, 2006; Barnes,  
60 2006; Albu et al., 2006; Carter, 2006; Rudzinski, 2006; Zielinska et al., 2006). Chamber simulations have  
61 irreplaceable advantages over other laboratory methods such as oxidation flow reactors (Kang et al.,  
62 2007; Lambe et al., 2015; Corral Arroyo et al., 2018; Cosman and Bertram, 2008) and bulk solution  
63 experiments (Brunamonti et al., 2015; Turšič et al., 2003; Pratap et al., 2021; Fleming et al., 2020; Mekić  
64 et al., 2019) in tracking atmospheric transformation processes and understanding kinetic processes.

65 The development of chambers is closely related to advances in atmospheric chemistry research. Starting  
66 with studies of photochemical smog in Los Angeles in the 1940s (Haagensmit, 1952) and continuing to  
67 the 1970s, chambers were designed primarily to study the formation of ozone (Akimoto et al., 1979;  
68 Carter et al., 1982) as well as the chemistry of volatile organic compounds (VOCs) and NO<sub>x</sub> (Morriss et  
69 al., 1957) in the atmospheric boundary layer. With the development of submicron particle measurement  
70 techniques, chambers were further used in secondary organic aerosol (SOA) formation studies from the  
71 1980s leading to numerous important scientific discoveries (Hidy, 2019; Odum et al., 1996; Odum et al.,  
72 1997; Griffin et al., 1999; Paulsen et al., 2005; Rollins et al., 2009; Hu et al., 2014; Wang et al., 2014).



73 Since the beginning of the 21<sup>st</sup> century, many chambers have been built or upgraded to address integrated  
74 atmospheric scientific questions, including PM<sub>2.5</sub> pollution (Johnson et al., 2004; Hallquist et al., 2009;  
75 Hurley et al., 2001), reaction kinetic parameters, mechanisms of VOC oxidation intermediates (Brauers  
76 et al., 2003; Bohn et al., 2004; Ren et al., 2017), as well as multiphase processes (Warneke and C., 2004;  
77 Pöschl and Shiraiwa, 2015; Liu and Abbatt, 2021; Franco et al., 2021).

78 In recent years, multiphase chemistries have been invoked to explain the bursting growth of particles (Su  
79 et al., 2016; Wang et al., 2016; Su et al., 2020) and physicochemical processes of SOA formation under  
80 high ion strength conditions in the atmosphere (Cheng et al., 2015; Su et al., 2020; Liu et al., 2021).  
81 Atmospheric multiphase processes can undergo different reaction pathways that are influenced by  
82 different environmental conditions (e.g., light, temperature, and relative humidity (RH)) and aerosol  
83 physicochemical properties including aerosol liquid water content (ALWC), aerosol phase state, and  
84 morphology (George and Abbatt, 2010; Davidovits et al., 2011; Abbatt et al., 2012; Ziemann and  
85 Atkinson, 2012; Herrmann et al., 2015; Ravishankara, 97; George et al., 2015; Su et al., 2020). Thus, a  
86 precise control of such parameters in a chamber system is vital for simulating atmospheric multiphase  
87 chemistry. Different from outdoor chambers (Leone et al., 2010; Stern et al., 1987; Pandis et al., 1991;  
88 Johnson et al., 2004; Martin-Reviejo and Wirtz, 2005; Rollins et al., 2009; Cocker et al., 2001; Peng et  
89 al., 2017), indoor chambers are usually equipped with artificial light sources (Takekawa et al., 2003;  
90 Carter et al., 2005; Paulsen et al., 2005), that can provide controllable irradiation for the simulation of  
91 multiphase processes. Compared to large chambers (Brauers et al., 2003; Leone et al., 1985; Pandis et  
92 al., 1991), temperature and RH inside small chambers can achieve faster equilibria and provide a more  
93 precise simulation of parameters such as diurnal RH change and ALWC (Takekawa et al., 2003; Carter  
94 et al., 2005; Paulsen et al., 2005; Wang et al., 2014; Bin Babar et al., 2016), thus improving  
95 reproducibility and efficiency when conducting experiments. Adversely, the wall loss effects are more  
96 significant for small chambers (Carter et al., 1982; Carter and Lurmann, 1991; Dodge, 2000). As studies  
97 showed evidence that the morphology and phase state of aerosol particles play important roles in the  
98 atmospheric multiphase chemistry processes (Virtanen et al., 2010; Berkemeier et al., 2016; Wang et al.,  
99 2015a; Reid et al., 2018), focused chamber studies on multiphase chemistry require additional steps to  
100 control the morphology and phase state of seed particles in chamber design (Faust et al., 2017; Zhou et  
101 al., 2019; Zhang et al., 2018; Zhang et al., 2019).

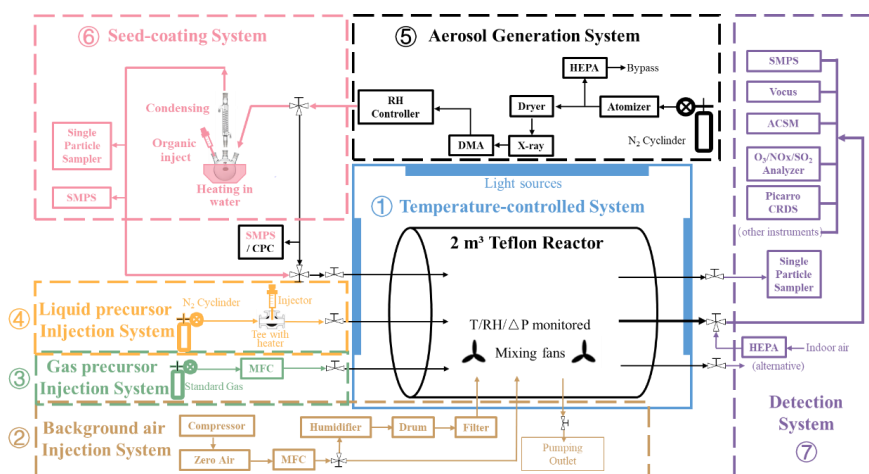
102 In this study, we designed and built a new indoor 2 m<sup>3</sup> Teflon chamber system (Aerosol multiphase



103 process Research chamber, AIR) with a focus on accurately simulating atmospheric multiphase processes.  
104 The temperature and RH inside the AIR chamber were precisely controlled to within  $\pm 0.15$  °C and  $\pm$   
105 0.75 %, respectively. A quantitative manipulation of the RH cycle was designed to simulate the diurnal  
106 variations in ambient RH. The seed generation subsystem, including an inorganic particle pre-  
107 deliquescence unit and an organic-coating unit, was designed to manipulate the aerosol phase state and  
108 organic-coated morphology. A series of experiments were conducted to characterize the spectral  
109 distribution and photolysis parameters of light sources, temperature, RH, wall loss behaviors of gas and  
110 particles, and particle morphology. Additionally, a series of experiments involving the oxidation of  $\alpha$ -  
111 pinene with seed particles were conducted in the AIR chamber to demonstrate the effectiveness of the  
112 chamber in simulating atmospheric multiphase chemistry.

## 113 **2 Facility**

114 Figure 1 displays the schematic design of AIR chamber system, and the real picture of the reactor bag  
115 and enclosure system are shown in Fig. S1. The chamber system includes the 2 m<sup>3</sup> fluorinated ethylene  
116 propylene (FEP) Teflon film (75  $\mu$ m, Du Pont, USA, light transmission  $\geq 93\%$ ) reactor and the associated  
117 temperature and RH control, artificial light sources, zero air injection and humidification, gaseous/liquid  
118 precursor injection, seed aerosol generation, and the instrument-optional detection components. To  
119 achieve a precise control of thermodynamic parameters and aerosol morphology when simulating  
120 atmospheric multiphase chemistry processes, the temperature inside the reactor is precisely controlled to  
121 within  $\pm 0.15$  °C. An RH regulation module is designed and built to simulate the ambient RH diurnal  
122 variation, which is capable of changing the RH in the reactor at a time scale of half an hour. In addition,  
123 a pre-deliquesting device and a coating device are custom-built to couple to the seed aerosol generation  
124 component, for manipulating the phase state (metastable aqueous or solid) and core-shell morphology  
125 (1 % ~ 12 % shell thickness) of seed aerosols. The detailed description of each system is shown in Section  
126 2.1-2.4.



127  
128

**Figure 1. Schematic diagram of AIR chamber system.**

129

## 2.1 The reactor and enclosure

130

The Teflon reactor is a 2 m<sup>3</sup> horizontal cylinder (1.2 m in diameter, 1.8 m in length). It is fixed on a stainless-steel frame with four ridges firmly adhered on the Teflon air bag (Fig. S1), so that the variable volume of the reactor during sampling is adequate (this chamber system is designed to operate in Batch Mode). As to each circle side of the cylinder, three stainless steel tubes are threaded through the Teflon film to act as the inlets (for injecting seeds and liquid phase precursors) or sampling outlets for the detection system, respectively. The interface between each tube and the film is sealed by a Teflon flange and a perfluorinated O-ring. At the bottom inside the reactor, two magnetic-levitation fans (patent number: 2019213329392, Beijing Convenient Environmental Tech Co. Ltd.) are equipped, with four speed levels (1000, 1350, 1700, 2000 rpm). A temperature and RH sensor (HMP110, Vaisala, Finland) and a differential pressure sensor (MSX-W10-PA-LCD, Dwyer, America) are also equipped at the bottom inside the reactor.

141

The rectangular enclosure (2.4 × 1.6 × 2.3 m, L, W, H) of the reactor is temperature-controlled by a circulation system. The indoor air is introduced from the top of the enclosure and exhausts through the bottom. The chiller power is constant, while the heating power is controlled through a proportional-integral-derivative (PID) feedback. Forty black lights (1.2 m, 40 W, Bulb-T12, GE, USA) are fixed on the inner wall of the enclosure as light sources for atmospheric process simulation. The number and position of these lights in work can be controlled by the system computer, so that the light intensity can be variable in experiments. Specular insulated material (SUS304, stainless steel, 8K, mirror plate) is used

147



148 as the enclosure inner wall so that the irradiation inside the reactor can be homogeneous. One side of the  
149 enclosure is a double door for entering and reactor maintenance.

## 150 **2.2 Cleaning and humidifying system**

151 The background gas in the reactor is from the indoor air. An air compressor (FOHUR, FH-50L)  
152 compresses the indoor air into a zero-air generator (Aadco, 737-14-A-CH4-240) for purification,  
153 removing airborne contaminants such as particulate matters, hydrocarbons, water vapor, NO<sub>x</sub>, O<sub>3</sub> and  
154 SO<sub>2</sub> to produce zero air (RH can be dried to < 2%, and the background concentrations of other  
155 contaminants are displayed in Table S2). Then, with the control of a mass flow controller (MFC,  
156 HORIBAMETRON, S4832/HMT), zero air is fed into the reactor through a 1/2" stainless steel tube  
157 (sealed at the bottom interface by a 304 stainless steel flange) at a flow rate of ≤ 50 L/min (to ensure the  
158 cleaning efficiency of the zero-air generator is sufficient), acting as the background gas and cleaning gas  
159 for the reactor. At the same time of feeding into the cleaning zero air, a pump beside the chamber system  
160 will exhaust the air from the reactor with a flow rate of 20 L/min to accelerate the gas exchange. The  
161 positive differential pressure inside the reactor is monitored. When the differential pressure reaches 30  
162 Pa, the MFC will stop the zero-air feed, and when the value falls below 20 Pa, zero air feed will restart.  
163 This is designed to avoid damaging the Teflon film of the reactor during cleaning.

164 The zero air is also used as humidifying gas. When switching to the humidification mode, the zero air  
165 will go into a humidification tank filled with deionized water (Milli-Q, 18MΩ) switched by a three-way  
166 valve, generating humidified zero air. Then, the humidified air flows through a filter (Waterman, HEPA)  
167 to remove the water droplet, and injects into the reactor to humidify. During the humidifying, the exhaust  
168 pump mentioned above keeps working. The flow rate of the humidified zero air (20 ~ 25 L/min) is set to  
169 be slightly higher than the exhausting rate for fast reaching the target RH inside the reactor.

## 170 **2.3 Precursor injection system**

171 According to the phase state of precursor reagents, the precursor injection system of this chamber system  
172 contains two types. One is used for the injection of gaseous precursors. Standard gas cylinders containing  
173 reactive gas (such as SO<sub>2</sub>, NO<sub>2</sub>, NH<sub>3</sub>, HCHO, etc.), inject relevant gaseous precursors into the reactor at  
174 a set flow rate and injecting duration under the control of a computer-connected MFC. The oxidant O<sub>3</sub> is  
175 produced through the decomposition of O<sub>2</sub> (from a standard O<sub>2</sub> cylinder) exposed to the 185 nm UV light.



176 After flowing through the MFC, the gaseous species enter the reactor via a stainless-steel tube at the  
177 bottom of the chamber.

178 The other type is used for the injection of liquid precursors. Note that, the liquid precursors here mean  
179 the species is in liquid phase before injected into the reactor, but should be gaseous after injecting into  
180 the chamber, such as  $\alpha$ -pinene standard solvent. A tee (the inlet on the left side of the chamber, as shown  
181 in the 'Liquid precursor Injection System' in Fig. 1) is fitted in the pipeline before the liquid precursors  
182 entering the reactor, with a 1 mm thick silicone membrane clamped to the right-angled end. The specific  
183 amount of the liquid precursors is taken with a microsyringe, penetrating the silicone membrane and  
184 slowly injected into the tee. At the same time, pure  $N_2$  is used as the carrier gas to vaporize the liquid  
185 precursor and carry it into the reactor under a specific gas cylinder pressure (0.25 MPa). After injection,  
186  $N_2$  is continuously purged for 60 seconds to ensure that no liquid precursors remain in the pipeline.

#### 187 **2.4 Seed generation system**

188 The seed aerosol generating system is a complex subsystem of AIR chamber system designed in this  
189 study. In addition to the common aerosol generation device, this study couples an RH-controlling device  
190 and a coating device to control the phase state and morphology of the seeds for supporting the simulation  
191 of atmospheric multiphase processes.

192 Commonly, the species used to generate the seed particles (typically dissolved inorganic salts such as  
193 ammonium sulfate and sodium chloride) are first dissolved in deionized water (Milli-Q, 18 M $\Omega$ ) and  
194 then generate a solution. Then, it is atomized as humid aerosol flow by an atomizer (TSI 3076) with  $N_2$   
195 blowing. Passing through a Nafion tube (PERMA PURE, MD-700-24F-3), the humid flow is dried and  
196 forms dry polydisperse seed aerosols. The drying is realized by pumping the air at the outer layer of the  
197 Nafion tube to a negative pressure ( $\sim 20$  kPa). It is tested that, within the range of the aerosol generation  
198 flow rate ( $\leq 3$  L/min), the RH of the aerosol flow can be dried to below 30 %. An X-ray neutralizer and  
199 DMA (DMA, Model 3082, TSI, Inc., USA) are optional, for selecting monodisperse aerosols from the  
200 polydisperse aerosol flow (flow rate ratio of sheath flow to aerosol flow is controlled between 5:1 and  
201 10:1), to support monodisperse experiments.

202 Besides, an RH controlling device is designed in this study to pre-deliquest the generated dry seeds that  
203 forming metastable seed aerosols. As shown in Fig. S9,  $N_2$  is used as the initial gas, which is then divided  
204 into two paths, one is the dry  $N_2$ , and the other goes through the deionized water (Milli-Q, 18M $\Omega$ , heated



205 to 45 °C) to act as the wet gas. The flow rate of each path is controlled by an MFC (GAS TOOL  
206 INSTRUMENT, GT 130MAX). Then the two flows mix into one as the humidifying gas and enter the  
207 outer layer of a Nafion semi-permeable tube (PERMA PURE, MD-700-24F-3). The flow with seed  
208 aerosols goes through the inner layer of the Nafion tube and then is humidified. The RH of the humidified  
209 flow is detected by an RH sensor (HYGROCLIP2, HC2A-S). The two MFCs of each flow path and the  
210 RH sensor are connected to a computer and controlled by a Labview program with PID feedback.  
211 Through the two MFCs adjusting the ratio of the flow rates of the dry and wet flow path, the RH of seed  
212 aerosol flow is controlled. This device has been tested to enable rapid changes in RH between 5 % and  
213 90% within 5 mins, and the RH variability can be within  $\pm 0.2$  %.

214 In order to investigate the effect of aerosol coating on atmospheric multiphase process, a device is  
215 designed in this study to generate a thickness-controlled and species-known coating on the generated dry  
216 monodisperse seed aerosols. The constitution of the coating device is shown in Fig. S10. This device  
217 consists of a water bath (Changfeng, HW.SY11-KP1), a three-necked flask (250 mL, 19#-24#-19#), a  
218 condensing glass tube (30 cm, 24#), and a thermostatic bath (BiLon, SC-05B). The organic species (~  
219 400  $\mu$ L) with low volatility (saturated vapor pressure in the order of  $10^{-4} \sim 10^{-5}$  mmHg at room  
220 temperature) used to form coating is set at the bottom of the three-necked flask, which is heated in the  
221 water bath to evaporate the organic vapor. The dried seed aerosol flow enters through the side port of the  
222 three-necked flask, and then carries the hot organic vapor into the condensing tube (condensing  
223 temperature is controlled at 20 °C by the thermostatic bath in this study). Due to the reduced temperature,  
224 the saturated vapor pressure of the organic drops, and the organic vapor will preferentially condense on  
225 the surface of seed aerosols that forming a coating.

## 226 **2.5 Detection system**

227 As shown in Figure 1, three stainless steel tubes are fixed on the right side of the reactor to act as sampling  
228 outlets. The middle steel tube of them is 3/8 " in size and acts as the main sampling tube, connected to a  
229 3/8 " stainless steel three-way plug valve. One outlet of the plug is attached to a HEPA filter, and the  
230 other outlet is attached to the line to sampling instruments. This design allows a quick sampling switch  
231 between indoor air and the reactor. The other two stainless steel tubes are both 1/4 " and are used as  
232 auxiliary sampling outlets (e.g. temporarily collect single particle samples for a few minutes).

233 An SMPS system (a DMA, Model 3082, and a CPC, Model 3772, TSI, Inc., USA), and a CPC (Model





234 3750, TSI, Inc., USA) downstream of the seed generation system, are the standing instruments for the  
235 chamber system, used to measure the particle number size spectrum distribution and particle total number  
236 concentration in the reactor, respectively. Other instruments are optional according to the specific  
237 research aim, and typically the total sampling flow rate should be lower than 6 L/min.

238 The other detection instruments involved in this study, include the instruments for gaseous species  
239 detection (Thermo Scientific gas analyzer (Model 43i-TLE for SO<sub>2</sub>, Model 42i-TL for NO<sub>x</sub>, Model 49i  
240 for O<sub>3</sub>, Model 48i-TLE for CO), Picarro cavity ring-down spectroscopy (Picarro CRDS, G2401) for CO<sub>2</sub>  
241 and CH<sub>4</sub>, Summa Canister (SILONITE, 1869) and GC-MS (Agilent, 7890A/5975C) for non-methane  
242 hydrocarbon (NMHC)), instruments for particulate species detection (Time-of-Flight Aerosol Chemical  
243 Speciation Monitor (ToF-ACSM, Aerodyne)), and instruments for volatile organic compounds (Vocus  
244 Proton-Transfer Reaction Time-Of-Flight Mass Spectrometry (Vocus-PTR-TOF-MS, Vocus S, Tofwerk),  
245 shorted as Vocus).

246 The sampling flow rate of each instrument is calibrated before each experiment. For Thermo Scientific  
247 instruments and Vocus, a single standard concentration is tested at each experiment, to act as a basis for  
248 instruments status verification and data quantification. For the data collected by ACSM, the calibration  
249 is performed based on the mass concentration calculated from SMPS data.

### 250 **3 Characterization of the AIR chamber**

251 A series of experiments were carried out to evaluate the performance of this chamber system, including  
252 leakproofness, sample-volume support, background concentrations, mixing performance, light  
253 characteristics, temperature and RH control, gas and particle wall loss, as well as characterizations of  
254 aerosol particles with the core-shell morphology. All the instruments for measurement are included in  
255 Section 2.5.

#### 256 **3.1 Fundamental parameters**

257 Leakproofness of the reactor was characterized by the positive pressure difference between the air inside  
258 the reactor and the ambient air and the change in the total number concentration of background particles  
259 inside the reactor. When the reactor was filled with zero air, the positive pressure difference inside the  
260 reactor was maintained at > 3 Pa for more than 25 hours (Fig. S2a), then slowly decreased to ~ 0.5 Pa  
261 after several days. When the air inside the reactor was sampled at a flow rate of 5 L/min, the positive



262 pressure difference decreased to zero after 2 hours, and then total particle number concentration slowly  
263 increased from  $\sim 0 \text{ cm}^{-3}$  to a final  $< 10 \text{ cm}^{-3}$  in  $\sim 3.5$  hours (Fig. S2b). This concentration is negligible for  
264 a particle number concentration of  $10^3 \sim 10^4 \text{ cm}^{-3}$  that are usually used in experiments. Moreover, this  
265 chamber system is designed to operate in batch mode, and the reactor can provide a sampling volume of  
266  $1000 \sim 1200 \text{ L}$  (Fig. S3) and a sampling time of more than 3 hours at a total sampling flow rate of  $5\sim 6$   
267  $\text{L/min}$ . The results above indicate that the system leakproofness is reliable for further experiments.

268 The reactor background was also characterized after repeated cleaning with zero air. As shown in Fig.  
269 S4, the background particle total number concentration was  $< 1 \text{ cm}^{-3}$ , and increased only to  $4 \text{ cm}^{-3}$  with  
270 the mixing fans turned on. Irradiation slightly increased the background particle concentration but still  
271 only to  $< 10 \text{ cm}^{-3}$ , which is negligible when compared with normal reaction conditions. Table S1 shows  
272 the background concentrations of chemical species in AIR chamber reactor under dry and high RH  
273 conditions. Compared with data reported for other chambers (White et al., 2018; Bin Babar et al., 2016;  
274 Wang et al., 2014; Platt et al., 2013; Carter et al., 2005; Chen et al., 2019b), the background  
275 concentrations of gaseous pollutants including  $\text{SO}_2$ ,  $\text{NO}_x$ ,  $\text{O}_3$  and  $\text{CO}$  in the reactor were comparable or  
276 lower for the AIR chamber. The background concentration of total non-methane hydrocarbon (NMHC)  
277 was higher than literature values due to the presence of chemically inert  $\text{CHClF}_2$  (half of the total NMHC  
278 concentration), which originates from the indoor refrigeration system and is hard to eliminate within the  
279 zero-air generation system. Nevertheless, this species does not interfere with the reactions under most  
280 experimental conditions. The reactor can be cleaned to background levels with a volume of zero air  $>5$   
281 times that of the reactor (Table S2) after each experiment. The cleaning process can be completed in less  
282 than 9 hours, as shown in Section 2.2.

283 The mixing performance of the injection into the reactor was examined using  $\text{NO}_2$  concentration and  
284 total particle number concentration as tracers (Fig. S5). The mixing time to uniformity was 5 minutes  
285 without running fans and less than 1 minute with the fans on. Furthermore, the mixing time was  
286 independent of the fan speed.

### 287 **3.2 Light source characterization**

288 The reflective inner wall (SUS304, stainless steel, 8K, mirror plate) of the AIR chamber is equipped with  
289 40 UV lamps (1.2 m, 40 W, Bulb-T12, GE, USA) to provide irradiation during the experiments. There  
290 are 10 lamps on the left, right, back, and top of the wall, respectively, and each lamp can be turned on or



291 off separately by the control system, so that the light intensity in experiments varies from 2.5% to 100%  
292 intensity. These light sources can also be replaced by lamps with different emission spectra to provide a  
293 variety of irradiation conditions.

294 For current light sources, a portable UV spectrometer (StellarNet Inc., Tampa FL, USA) was used to  
295 characterize the irradiance spectrum in the reactor (Fig. S6). The irradiance is mainly distributed in the  
296 range of 360 ~ 390 nm, peaking at 370 nm, which is within the range of peak irradiance of UV lights  
297 used in other indoor chambers (340 ~ 371 nm) (Wang et al., 2014; Ma et al., 2022; Bin Babar et al., 2016;  
298 Chen et al., 2019b; Lane and Tang, 1994; Thuner et al., 2004). Another small peak appears at 405 nm,  
299 which is convenient for directly checking the status of the lamps.

300 The photolytic rate constant for NO<sub>2</sub> can be used to characterize the irradiation intensity. Previous  
301 literature (Wang et al., 2014; Bin Babar et al., 2016; Ma et al., 2022) often characterize irradiation  
302 intensity through the photolytic rate constant of NO<sub>2</sub> ( $J_{\text{NO}_2}$ ), calculated through the steady-state  
303 concentrations of NO<sub>x</sub> and O<sub>3</sub> (Atkinson et al., 2004). This study mainly used a spectrometer, namely  
304 the Jvalue instrument (AVANTES, AvaSpec-ULS-TEC-EVO), to measure the irradiance and directly  
305 calculate the photolytic rate constants of a few important species in atmospheric photochemistry. Notably,  
306 the Jvalue instrument was also calibrated using the  $J_{\text{NO}_2}$  values derived from the steady NO<sub>x</sub>-O<sub>3</sub>  
307 concentration under several light schemes to correct for the geometry defect of the Jvalue instrument  
308 when placed inside the AIR chamber. The calibration factor of the traditional  $J_{\text{NO}_2}$  method is  $1.49 \pm$   
309  $0.06$ . As shown in Table S3, the current light source is more suitable for the photolysis of HONO and  
310 NO<sub>2</sub> (photolytic rate constants on the order of  $10^{-4} \sim 10^{-3} \text{ s}^{-1}$ ). However, the photolysis of HCHO, H<sub>2</sub>O<sub>2</sub>,  
311 and O<sub>3</sub> is slow (photolytic rate constants on the order of  $10^{-8} \sim 10^{-7} \text{ s}^{-1}$ ). The  $J_{\text{NO}_2}$  maxima of other  
312 chambers are usually in the range of  $2 \sim 9 \times 10^{-3} \text{ s}^{-1}$  (Chen et al., 2019a; Li et al., 2017; Wang et al., 2014;  
313 Bin Babar et al., 2016; Ma et al., 2022). In comparison,  $J_{\text{NO}_2}$  due to the light source in the AIR chamber  
314 is  $4.10 \times 10^{-3} \text{ s}^{-1}$ , close to the median value of the other chambers. Moreover, the photolytic rate constant  
315 of HONO due to the light source in this chamber ( $J_{\text{HONO}}$  at the level of  $10^{-4} \text{ s}^{-1}$ ) is comparable to or  
316 slightly higher than the value of HONO photolysis in the ambient atmosphere in China ( $J_{\text{HONO}}$  at the  
317 level of  $10^{-5} \sim 10^{-4} \text{ s}^{-1}$ ) (Zheng et al., 2020).

318 When only lamps on two sides of the AIR chamber were turned on (four schemes with 20 lights on, noted  
319 as ‘only back/top’, ‘left and right’, ‘odd’ and ‘even’ in Table S3), the photolytic rate constants in the  
320 reactor under different configurations were almost the same ( $J_{\text{HONO}} = 5.10 \pm 0.12 \times 10^{-4} \text{ s}^{-1}$ ,  $J_{\text{NO}_2} =$



321  $2.16 \pm 0.05 \times 10^{-3} \text{ s}^{-1}$ ), and nearly equal to half of that with all 40 lights on. In addition, the photolytic  
322 rate constant of the scheme ‘left and right’ (40 lights) was the sum of that of ‘only left’ (20 lights) and  
323 ‘only right’ (20 lights). These results indicate that the irradiation in the reactor is uniformly distributed.  
324 Notably, because the measurement interface of Jvalue was a little biased to the left during detection, the  
325 value for ‘only left’ was higher than that for ‘only right’.

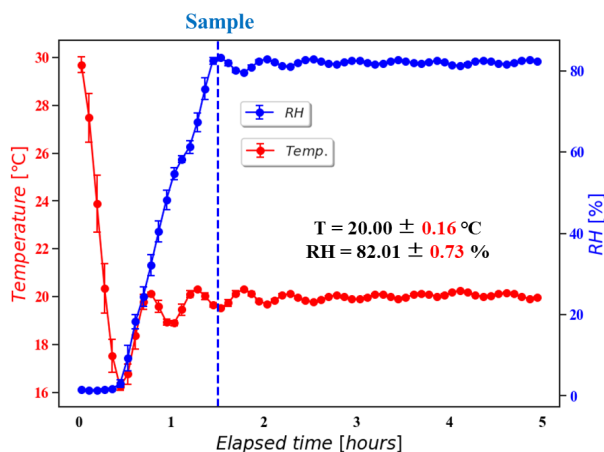
### 326 **3.3 Performance of temperature and RH control**

327 The temperature and RH in the reactor are measured by a high-accuracy sensor (HMP110, Vaisala,  
328 Finland). Detailed descriptions of temperature and RH control are given in Section 2.1 and 2.2. The  
329 accuracy for RH of this sensor is shown by its measurement error of  $< 1\%$  from that measured by a  
330 hygrometer (chilled mirror hygrometer, Edgetech Instrument, USA), with an  $R^2 > 0.99$ . The temperature  
331 in the reactor can be stably controlled in the range of  $2.5 \text{ }^\circ\text{C} \sim 31 \text{ }^\circ\text{C}$ , and the control range of RH is  $< 2\%$   
332  $\sim 95\%$ . The fluctuations in the temperature inside the reactor are within  $\pm 0.15 \text{ }^\circ\text{C}$  of any set temperature,  
333 and the corresponding RH fluctuations for  $\text{RH} > 80 \%$  are within  $\pm 0.75 \%$ . The stability achieved with  
334 the temperature and RH controls across a wide range of temperatures is shown in Table S4. The  
335 illumination of lamps raises the lowest achievable temperature by  $3 \text{ }^\circ\text{C}$  for every 10 lights on. However,  
336 the illumination of the reactor does not affect the stability of temperature and RH inside the reactor. When  
337 the set temperature is close to room temperature ( $20 \text{ }^\circ\text{C}$  in Table S4), the fluctuation is  $< 0.1 \text{ }^\circ\text{C}$ ,  
338 demonstrating a more accurate temperature and RH control performance compared with other chambers  
339 (Table S5) (Wang et al., 2014; Wu et al., 2007; Bin Babar et al., 2016; Ma et al., 2022; Wang et al.,  
340 2015b). Sampling operation (lasting more than 3 hours with flow rate at  $5 \text{ L/min}$ , Fig. 2) does not  
341 significantly affect the stability of temperature and RH control either, which also indicates the permeation  
342 and wall loss of water molecules do not affect a lot.

343 In order to simulate the diurnal variations in ambient air temperature and RH, a proportional-integral-  
344 derivative (PID) feedback controlling function was designed. The RH in the reactor can reach the target  
345 RH by controlling the temperature. After receiving the target RH input, the control program calculates  
346 the stepwise theoretical RH value at each time increment and the corresponding temperature control steps  
347 based on current temperature and RH in the reactor. This calculation is also adjusted in real-time to  
348 optimize the gradual change of RH. Figure S7 demonstrates two examples to show alternate linear change  
349 and constant control of RH. The RH can reach the set value within a few hours with fluctuations  $< 0.75\%$ .



350 This function performs even better at low temperatures, suggesting the potential of using this chamber  
351 system to simulate diurnal variations of RH in the ambient atmosphere in wintertime.



352  
353 **Figure 2. Stability of temperature and RH control in the reactor during sampling.**

### 354 3.4 Wall loss of gas and particles

355 The wall loss process is considered as a first-order kinetic process, in that the decay rate of a  
356 concentration is proportional to the concentration:

$$357 \frac{dC(t)}{dt} = -k * C(t) \quad (1)$$

358 where  $C(t)$  is the species concentration at time  $t$ , and  $k$  is the wall loss rate constant (in units:  $s^{-1}$  or  $min^{-1}$ ).  
359 The wall loss rates of gaseous species such as  $NO_x$  and  $O_3$  in this study are shown in Table S6, the  
360 values of which are lower than other small Teflon chambers ( $2 \sim 5 \text{ m}^3$ ) (Wu et al., 2007; Wang et al.,  
361 2015b; Li et al., 2017; Bernard et al., 2016), as a result of passivation of the inner surface of the reactor  
362 with 2 ppm  $O_3$  for 3 days.

363 The wall loss rate constant  $k$  of particles is dependent on particle size (diameter, noted as  $D_p$ ). Smaller or  
364 larger particles often have higher  $k$  values (Crump and Seinfeld, 1981) due to higher diffusion or  
365 sedimentation rates, respectively. The dependence of  $k$  values for particles with  $D_p < 50 \text{ nm}$  is rarely  
366 reported in previous chamber studies. This study demonstrates that the constant  $k$  decreases as a function  
367 of decreasing  $D_p$  when particles are smaller than 50 nm, which is also shown in Fig. S7 of Ma et al (Ma  
368 et al., 2022). The  $\log_{10}(k)$  value for particles can be approximated with a segmented linear function of  
369  $\log_{10}(D_p)^{93, 94}$ . In addition to the slopes to be determined, the inflection point  $D_p$ , where the loss trend



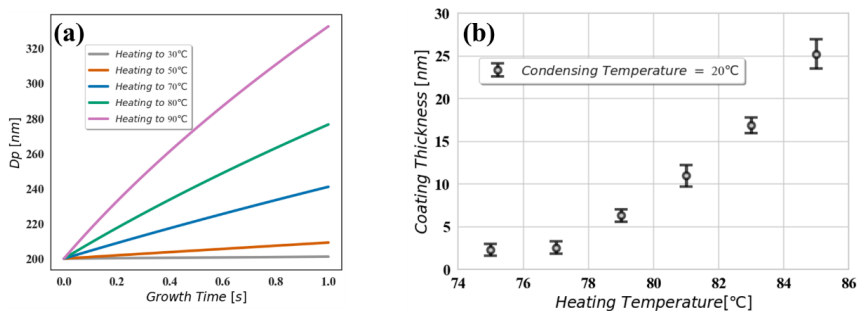
370 inverses, changes with different chambers. In this study, two inflection points are identified at 50 nm and  
371 150 nm (Fig. S8). Furthermore, the  $k$ - $D_p$  dependence has been reported to deviate in different  
372 experiments even in the same reactor. This study found that such deviations can be corrected through an  
373 up-and-down shift of the  $\log_{10}(k)$ - $\log_{10}(D_p)$  function curve. Even for deliquescent particles ( $RH = 90\%$   
374 in Fig. S8, the  $D_p$  of the x-axis represents the liquid particle diameters), this method still accurately  
375 described the relationship between  $k$  and  $D_p$  ( $R^2 \sim 0.95$ ) when considering the hygroscopic growth of the  
376 particle size.

377 Another commonly used parameter to characterize the particle wall loss behavior in chambers is the total  
378 volume wall loss rate constant ( $k_v$ ). For small Teflon chambers of  $2 \sim 3 \text{ m}^3$  in size (Takekawa et al., 2003;  
379 Li et al., 2017; Liu et al., 2019),  $k_v$  values typically range from  $2.84 \sim 4.72 \times 10^{-3} \text{ min}^{-1}$ . The particle wall  
380 loss is slightly higher in the chamber in this study, with the  $k_v$  found to be  $5 \times 10^{-3} \text{ min}^{-1}$  (Table S7).

### 381 **3.5 Morphology of seed particle generation**

382 Seed particles are typically used to simulate aerosol formation by the multiphase chemistry pathway. The  
383 AIR chamber is designed to couple to a subsystem for generating seed particles with different phase  
384 states through pre-deliqescing, adopted from a previous study (Faust et al., 2017). A volatilizing-  
385 condensing method is used to generate known-composition organic-coated inorganic particles in the AIR  
386 chamber, with a detailed description in Section 2.4.

387 As shown in Figure 3, squalane is coated onto dry 200-nm monodisperse NaCl seed particles to produce  
388 a core-shell morphology for the particles. The coating thickness is controlled by adjusting the water bath  
389 heating temperature while maintaining a fixed condensation temperature of  $20 \text{ }^\circ\text{C}$ . Using the Clausius-  
390 Clapeyron equation that describes the relationship between saturation vapor pressure and temperature,  
391 as well as the Maxwell equation that describes the condensation growth rate of particle size under a  
392 certain supersaturated vapor pressure, the coating thickness can be predicted in relation to the heating  
393 temperature (Fig. 3a), to assess the feasibility of the selected coating species. The coating thickness is  
394 calculated as half of the difference in peak  $D_p$  of the monodisperse particle size distribution before and  
395 after the seeds are coated (Fig. 3b). For squalane, the device allows for a relatively accurate control of  
396 coating thickness in the range of 5 to 25 nm (1% ~ 12% shell thickness). For organic species with similar  
397 volatilities (saturated vapor pressure in the order of  $10^{-4} \sim 10^{-5} \text{ mmHg}$  at room temperature), the device  
398 could provide similar control performance.



399

400 **Figure 3. Relationship between coating thickness on dry 200 nm NaCl seed and heating temperature in the**  
 401 **coating device, with squalane as the coating species and 20 °C condensing temperature. (a) Theoretical**  
 402 **estimation in different growth times. (b) Measured results by SMPS.**

#### 403 4 Applications in SOA generation— $\alpha$ -pinene ozonolysis researches

##### 404 4.1 SOA yield of seed-absent experiments

405 SOA are generated from  $\alpha$ -pinene ozonolysis in the AIR chamber to evaluate its performance, with  
 406 experiment conditions given in Table S8 (NO.1 ~ 5). The key parameter Y, representing the yield of SOA,  
 407 is defined as:

$$408 \quad Y = \frac{\Delta mo}{\Delta ROG} \quad (2)$$

409 where  $\Delta mo$  represents the total mass concentration of generated SOA, and  $\Delta ROG$  represents the total  
 410 mass concentration of reactive organic gas that was consumed in the reaction (specifically referring to  $\alpha$ -  
 411 pinene in this study), with both units in  $\mu\text{g}/\text{m}^3$ . SOA mass concentration was measured by a ToF-ACSM  
 412 (Section 2.5). The organic mass measurement was also corrected based on the particle size distribution  
 413 data from SMPS, where the  $\alpha$ -pinene-derived SOA density was assumed as  $1.3 \text{ g}/\text{cm}^3$ . This density value  
 414 is also used in many previous researches (Bahreini et al., 2005; Alfarra et al., 2006; Ma et al., 2022), but  
 415 higher than the unit density assumption used in some other chamber studies (Wang et al., 2011; Wang et  
 416 al., 2014; Bin Babar et al., 2016; Cocker Iii et al., 2001; Li et al., 2021; Zhang et al., 2015).

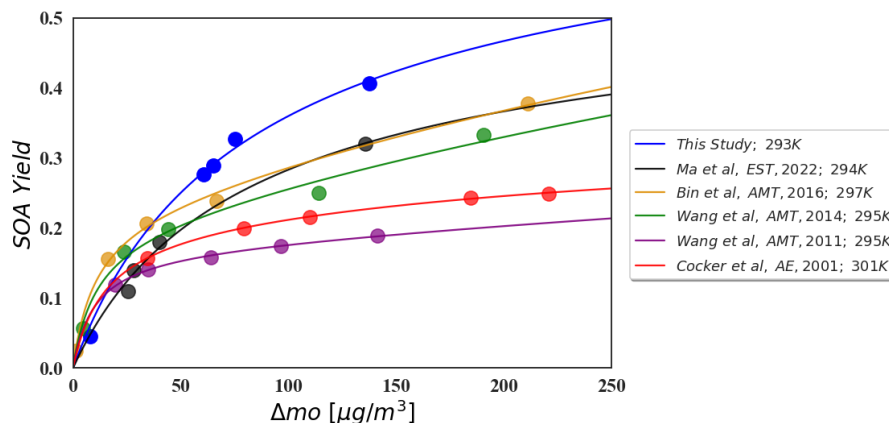
417 Odum et al (Odum et al., 1996) found that the two-product model reproduces well the non-linear  
 418 relationship between the SOA yield Y and the particulate organic mass concentration ( $mo$ ):

$$419 \quad Y = mo * \sum \frac{\alpha_i * K_{om,i}}{1 + mo * K_{om,i}} \quad (3)$$

420 where  $\alpha_i$  and  $K_{om,i}$  are the mass-based stoichiometric and partition coefficient for species i, respectively,  
 421 and  $mo$  is the total mass concentration of organic aerosol. Figure 4 shows the results of the two-product



422 model that fits the seed-absent SOA yield results in this study. The Odum model fits results from other  
423 chamber studies are also shown in Figure 4 for comparison. Detailed model fitting parameters are shown  
424 in Table S9. In contrast,  $Y$  in this study is a little higher than those in other small or medium-sized  
425 chambers, which may be owing to the lower gas wall loss in our Teflon reactor (Section 3.4). The four  
426 fitting parameters in this study,  $\alpha_1$ ,  $\alpha_2$ ,  $K_1$ ,  $K_2$ , are 0.62479, 0.0326791, 0.0121589, 0.0121596,  
427 respectively.  $K_1$  and  $K_2$  are close and are moderate values; however,  $\alpha_1$  is significantly higher than those  
428 in other chambers. Such higher value for  $\alpha_1$  can be an indication of a lower volatilizing loss of the gas  
429 phase intermediates within the AIR reactor compared with the other chambers. The good fitting from our  
430 experiment indicates that the chamber system in this study is stable. These results imply a reliable  
431 performance of our chamber system for experimental simulation studies of atmospheric secondary  
432 transformation process.



433  
434 **Figure 4.** Two-product model fitting curve of seed-absent  $\alpha$ -pinene-derived SOA yield in this study and the  
435 comparison with other literature results. The data of the blue line is from this study, and other data is obtained  
436 from these references (Cocker Iii et al., 2001; Wang et al., 2011; Wang et al., 2014; Bin Babar et al., 2016; Ma  
437 et al., 2022).

#### 438 4.2 Effects of seed phase state on SOA yield

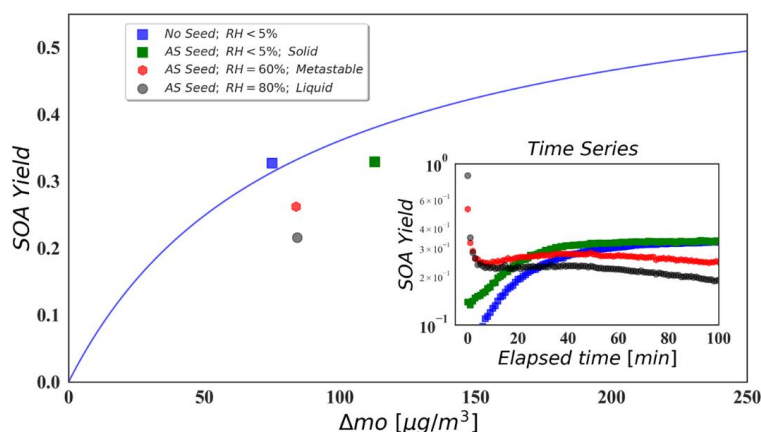
439 The effects of different seed phase state on the yield of  $\alpha$ -pinene-derived SOA were further investigated  
440 using ammonium sulfate as the seed particles (Table S8, NO.6 ~ 8). Figure S11 shows the relevant  
441 measured parameters during one reaction (e.g., experiment NO.8). The yields of all the experiments are  
442 summarized in Fig. 5. In general, the yield in the presence of dry seeds is not significantly different from  
443 that in the absence of seeds, consistent with the outcome of Odum et al (Odum et al., 1996). However,





444 in the presence of aerosol liquid water and ammonium sulfate seeds, the  $\alpha$ -pinene-derived SOA yield is  
445 reduced. This suppressing phenomenon is also reported by Cocker et al (Cocker Iii et al., 2001), which  
446 may be related to the finding of Lutz et al (Lutz et al., 2019) that an inhibition of organic species  
447 partitioning in the particulate phase exists at high sulfates level. However, to our knowledge, the  
448 suppressing phenomenon above may not be common, that has only been reported in the  $\alpha$ -pinene  
449 ozonolysis system with ammonium sulfate seeds.

450 The subplot in Fig. 5 demonstrates the SOA yield at each elapsed time point in these experiments. Liquid  
451 water can significantly promote the initial SOA yield and generation rate (Zhang et al., 2018), and our  
452 results have reproduced this phenomenon (subplot in Fig. 5). However, the oxidation reaction proceeds,  
453 it is observed that the SOA yield with liquid seeds decreases, and larger seed aerosol liquid water contents  
454 produce greater decreases in the yield. These indicate the AIR chamber system facilitates the researches  
455 of aerosol properties on atmospheric multiphase processes.



456  
457 **Figure 5.** Effects of phase state and liquid water content of ammonium sulfate seed particles on the SOA yield  
458 of  $\alpha$ -pinene ozonolysis ( $\alpha$ -pinene =  $60 \pm 13$  ppb, O<sub>3</sub> =  $296 \pm 30$  ppb). In the main plot, the blue line is the fitting  
459 two-product curve from no-seed experiments data in this study, which is a replicate of the curve in Fig. 4. The  
460 subplot shows the current yield since the initial time point of each experiment, where the blue points represent  
461 the data of no-seed experiment, green points represent the data of solid seed experiment, red points represent  
462 the data of metastable seed experiment, and grey points represent the data of liquid seed experiment.

## 463 5 Conclusions

464 The reported special phenomena relying on specific particle properties are well reproduced in AIR



465 chamber benefitting from the seed phase state control, and the accurate temperature and RH control  
466 facilitates the quantization of the effects of aerosol liquid water. Besides, compared to other chambers,  
467 the manipulation of composition and thickness of organic coating could provide a more clarity surface  
468 property. Broad temperature range, adjustable irradiation intensity, and the fast-responding RH cycle,  
469 make this chamber system suitable for simulating diurnal ambient atmosphere in different seasons. These  
470 performances of handling key parameters suggest the potential of this AIR chamber system for the  
471 laboratory simulation of atmospheric multiphase processes.

#### 472 **Data availability**

473 The data in this study are available from the authors upon request ([zhijunwu@pku.edu.cn](mailto:zhijunwu@pku.edu.cn)).

#### 474 **Acknowledgements**

475 We thank the Beijing Convenient Environmental Tech Co. Ltd. for constructing the chamber.

#### 476 **Financial support**

477 This research was financially supported by the National Natural Science Foundation of China  
478 (41875149).

#### 479 **Author contributions**

480 TZ and ZW conceived the study. TZ, ZW, JW, WF conducted the laboratory measurements. TZ carried  
481 out the data analysis. TZ, KB, YY, XY, ZB, XM, YZ participated in the instrument managements. SG,  
482 YC, CL, YZ, S-ML and MH supported this research. TZ wrote the paper with inputs from all co-authors.

#### 483 **Competing interest**

484 The authors declare that they have no known competing financial interests or personal relationships that  
485 could have appeared to influence the work reported in this paper.



486 **References**

- 487 Abbatt, J. P., Lee, A. K., and Thornton, J. A.: Quantifying trace gas uptake to tropospheric aerosol: recent  
488 advances and remaining challenges, *Chemical Society reviews*, 41, 6555-6581, 10.1039/c2cs35052a,  
489 2012.
- 490 Akimoto, H., Hoshino, M., Inoue, G., Sakamaki, F., Washida, N., and Okuda, M.: Design and  
491 characterization of the evacuable and bakable photochemical smog chamber, *Environ.sci.technol*, 13,  
492 471-475, 1979.
- 493 Albu, M., Barnes, I., and Mocanu, R.: Kinetic Study of the Temperature Dependence of the OH Initiated  
494 Oxidation of Dimethyl Sulphide, *Dordrecht*, 223-230,
- 495 Alfara, M. R., Paulsen, D., Gysel, M., Garforth, A. A., Dommen, J., Prevot, A. S. H., Worsnop, D. R.,  
496 Baltensperger, U., and Coe, H.: A mass spectrometric study of secondary organic aerosols formed from  
497 the photooxidation of anthropogenic and biogenic precursors in a reaction chamber, *Atmospheric  
498 Chemistry And Physics*, 6, 5279-5293, 2006.
- 499 Atkinson, R., Baulch, D. L., Cox, R. A., Crowley, J. N., Hampson, R. F., Hynes, R. G., Jenkin, M. E.,  
500 Rossi, M. J., and Troe, J.: Evaluated kinetic and photochemical data for atmospheric chemistry: Volume  
501 I - gas phase reactions of O-x, HOx, NOx and SOx species, *Atmospheric Chemistry And Physics*, 4,  
502 1461-1738, 2004.
- 503 Bahreini, R., Keywood, M. D., Ng, N. L., Varutbangkul, V., Gao, S., Flagan, R. C., Seinfeld, J. H.,  
504 Worsnop, D. R., and Jimenez, J. L.: Measurements of secondary organic aerosol from oxidation of  
505 cycloalkenes, terpenes, and m-xylene using an Aerodyne aerosol mass spectrometer, *Environmental  
506 Science & Technology*, 39, 5674-5688, 2005.
- 507 Barnes, I.: Kinetics, Products and Mechanism of O(3P) Atom Reactions with Alkyl Iodides,  
508 *Environmental Simulation Chambers: Application to Atmospheric Chemical Processes*2006.
- 509 Batchvarova, E., Spassova, T., Valkov, N., and Iordanova, L.: Survey on Atmospheric Chemistry  
510 Research in Some New EU Member States and Candidate Countries, *Dordrecht*, 301-340,
- 511 Bejan, I., Barnes, I., Olariu, R., Becker, K. H., and Mocanu, R.: FT-IR Kinetic Study on the Gas-Phase  
512 Reactions of the OH Radical with a Series of Nitroaromatic Compounds, *Dordrecht*, 155-162,
- 513 Berkemeier, T., Steimer, S. S., Krieger, U. K., Peter, T., Poschl, U., Ammann, M., and Shiraiwa, M.:  
514 Ozone uptake on glassy, semi-solid and liquid organic matter and the role of reactive oxygen  
515 intermediates in atmospheric aerosol chemistry, *Physical chemistry chemical physics : PCCP*, 18, 12662-  
516 12674, 10.1039/c6cp00634e, 2016.
- 517 Bernard, F., Ciuraru, R., Boreave, A., and George, C.: Photosensitized Formation of Secondary Organic  
518 Aerosols above the Air/Water Interface, *Environmental Science & Technology*, 50, 8678-8686, 2016.
- 519 Bin Babar, Z., Park, J. H., Kang, J., and Lim, H. J.: Characterization of a Smog Chamber for Studying  
520 Formation and Physicochemical Properties of Secondary Organic Aerosol, *Aerosol Air Qual Res*, 16,  
521 3102-3113, 2016.
- 522 Bohn, B., Rohrer, F., Brauers, T., and Wahner, A.: Actinometric measurements of NO<sub>2</sub> photolysis  
523 frequencies in the atmosphere simulation chamber SAPHIR, *ATMOSPHERIC CHEMISTRY AND  
524 PHYSICS*, 5, 493-503, 2004.
- 525 Brauers, T., Bohn, B., Johnen, F.-J., Rohrer, R., Rodriguez Bares, S., Tillmann, R., and Wahner, A.: The  
526 atmosphere simulation chamber SAPHIR: a tool for the investigation of photochemistry, April 01,  
527 20032003.
- 528 Brunamonti, S., Krieger, U. K., Marcolli, C., and Peter, T.: Redistribution of black carbon in aerosol  
529 particles undergoing liquid-liquid phase separation, *Geophysical Research Letters*, 42, 2532-2539, 2015.



- 530 Carter, W. P. L.: Environmental Chamber Studies of Ozone Formation Potentials of Volatile Organic  
531 Compounds, Dordrecht, 231-240,
- 532 Carter, W. P. L. and Lurmann, F. W.: Evaluation Of a Detailed Gas-Phase Atmospheric Reaction-  
533 Mechanism Using Environmental Chamber Data, *Atmos Environ a-Gen*, 25, 2771-2806, 1991.
- 534 Carter, W. P. L., Atkinson, R., Winer, A. M., and Pitts, J. N.: Experimental Investigation Of Chamber-  
535 Dependent Radical Sources, *International Journal Of Chemical Kinetics*, 14, 1071-1103, 1982.
- 536 Carter, W. P. L., Cocker, D. R., Fitz, D. R., Malkina, I. L., Bumiller, K., Sauer, C. G., Pisano, J. T.,  
537 Bufalino, C., and Song, C.: A new environmental chamber for evaluation of gas-phase chemical  
538 mechanisms and secondary aerosol formation, *Atmospheric Environment*, 39, 7768-7788, 2005.
- 539 Chen, B. B. and Lelevkin, V. M.: Influence of Atmospheric Aerosol Contamination on the Regional  
540 Climate in Central Asia, Dordrecht, 403-414,
- 541 Chen, T. Z., Liu, Y. C., Liu, C. G., Liu, J., Chu, B. W., and He, H.: Important role of aromatic  
542 hydrocarbons in SOA formation from unburned gasoline vapor, *Atmospheric Environment*, 201, 101-  
543 109, 2019a.
- 544 Chen, T. Z., Liu, Y. C., Ma, Q. X., Chu, B. W., Zhang, P., Liu, C. G., Liu, J., and He, H.: Significant  
545 source of secondary aerosol: formation from gasoline evaporative emissions in the presence of SO<sub>2</sub> and  
546 NH<sub>3</sub>, *Atmospheric Chemistry And Physics*, 19, 8063-8081, 2019b.
- 547 Cheng, Y., Su, H., Koop, T., Mikhailov, E., and Poschl, U.: Size dependence of phase transitions in  
548 aerosol nanoparticles, *Nature communications*, 6, 5923, 10.1038/ncomms6923, 2015.
- 549 Cocker, D. R., Flagan, R. C., and Seinfeld, J. H.: State-of-the-art chamber facility for studying  
550 atmospheric aerosol chemistry, *Environmental Science & Technology*, 35, 2594-2601, 2001.
- 551 Cocker Iii, D. R., Clegg, S. L., Flagan, R. C., and Seinfeld, J. H.: The effect of water on gas-particle  
552 partitioning of secondary organic aerosol. Part I:  $\alpha$ -pinene/ozone system, *Atmospheric Environment*, 35,  
553 6049-6072, [https://doi.org/10.1016/S1352-2310\(01\)00404-6](https://doi.org/10.1016/S1352-2310(01)00404-6), 2001.
- 554 Corral Arroyo, P., Bartels-Rausch, T., Alpert, P. A., Dumas, S., Perrier, S., George, C., and Ammann, M.:  
555 Particle-Phase Photosensitized Radical Production and Aerosol Aging, *Environ Sci Technol*, 52, 7680-  
556 7688, 10.1021/acs.est.8b00329, 2018.
- 557 Cosman, L. M. and Bertram, A.: Reactive Uptake of N<sub>2</sub>O<sub>5</sub> on Aqueous H<sub>2</sub>SO<sub>4</sub> Solutions Coated  
558 with 1-Component and 2-Component Monolayers, *Journal of Physical Chemistry A*, 112, 4625, 2008.
- 559 Crump, J. G. and Seinfeld, J. H.: Turbulent Deposition And Gravitational Sedimentation Of an Aerosol  
560 In a Vessel Of Arbitrary Shape, *Journal Of Aerosol Science*, 12, 405-415, 1981.
- 561 Davidovits, P., Kolb, C. E., Williams, L. R., Jayne, J. T., and Worsnop, D. R.: Update 1 of: Mass  
562 Accommodation and Chemical Reactions at Gas-Liquid Interfaces, *Chemical reviews*, 111,  
563 10.1021/cr100360b, 2011.
- 564 Dodge, M. C.: Chemical oxidant mechanisms for air quality modeling: critical review, *Atmospheric  
565 Environment*, 34, 2103-2130, 2000.
- 566 Faust, J. A., Wong, J. P., Lee, A. K., and Abbatt, J. P.: Role of Aerosol Liquid Water in Secondary Organic  
567 Aerosol Formation from Volatile Organic Compounds, *Environ Sci Technol*, 51, 1405-1413,  
568 10.1021/acs.est.6b04700, 2017.
- 569 Fleming, L. T., Lin, P., Roberts, J. M., Selimovic, V., Yokelson, R., Laskin, J., Laskin, A., and Nizkorodov,  
570 S. A.: Molecular composition and photochemical lifetimes of brown carbon chromophores in biomass  
571 burning organic aerosol, *Atmospheric Chemistry And Physics*, 20, 1105-1129, 2020.
- 572 Franco, B., Blumenstock, T., Cho, C., Clarisse, L., Clerbaux, C., Coheur, P. F., De Maziere, M., De Smedt,  
573 I., Dorn, H. P., Emmerichs, T., Fuchs, H., Gkatzelis, G., Griffith, D. W. T., Gromov, S., Hannigan, J. W.,



- 574 Hase, F., Hohaus, T., Jones, N., Kerkweg, A., Kiendler-Scharr, A., Lutsch, E., Mahieu, E., Novelli, A.,  
575 Ortega, I., Paton-Walsh, C., Pommier, M., Pozzer, A., Reimer, D., Rosanka, S., Sander, R., Schneider,  
576 M., Strong, K., Tillmann, R., Van Roozendaal, M., Vereecken, L., Vigouroux, C., Wahner, A., and  
577 Taraborrelli, D.: Ubiquitous atmospheric production of organic acids mediated by cloud droplets, *Nature*,  
578 593, 233-237, 10.1038/s41586-021-03462-x, 2021.
- 579 George, C., Ammann, M., D'Anna, B., Donaldson, D. J., and Nizkorodov, S. A.: Heterogeneous  
580 photochemistry in the atmosphere, *Chemical reviews*, 115, 4218-4258, 10.1021/cr500648z, 2015.
- 581 George, I. J. and Abbatt, J. P.: Heterogeneous oxidation of atmospheric aerosol particles by gas-phase  
582 radicals, *Nature chemistry*, 2, 713-722, 10.1038/nchem.806, 2010.
- 583 Griffin, R. J., Cocker, D. R., Flagan, R. C., and Seinfeld, J. H.: Organic aerosol formation from the  
584 oxidation of biogenic hydrocarbons, *Journal Of Geophysical Research-Atmospheres*, 104, 3555-3567,  
585 1999.
- 586 Haagensmit, A. J.: Chemistry And Physiology Of Los-Angeles Smog, *Industrial And Engineering*  
587 *Chemistry*, 44, 1342-1346, 1952.
- 588 Hallquist, M., Wenger, J. C., Baltensperger, U., Rudich, Y., Simpson, D., Claeys, M., Dommen, J.,  
589 Donahue, N. M., George, C., Goldstein, A. H., Hamilton, J. F., Herrmann, H., Hoffmann, T., Iinuma, Y.,  
590 Jang, M., Jenkin, M. E., Jimenez, J. L., Kiendler-Scharr, A., Maenhaut, W., McFiggans, G., Mentel, T.  
591 F., Monod, A., Prevot, A. S. H., Seinfeld, J. H., Surratt, J. D., Szmigielski, R., and Wildt, J.: The formation,  
592 properties and impact of secondary organic aerosol: current and emerging issues, *Atmospheric Chemistry*  
593 *And Physics*, 9, 5155-5236, 2009.
- 594 Herrmann, H., Schaefer, T., Tilgner, A., Styler, S. A., Weller, C., Teich, M., and Otto, T.: Tropospheric  
595 aqueous-phase chemistry: kinetics, mechanisms, and its coupling to a changing gas phase, *Chemical*  
596 *reviews*, 115, 4259-4334, 10.1021/cr500447k, 2015.
- 597 Hidy, G. M.: Atmospheric Chemistry in a Box or a Bag, *Atmosphere-Basel*, 10, 401, 2019.
- 598 Hu, C. J., Cheng, Y., Pan, G., Gai, Y. B., Gu, X. J., Zhao, W. X., Wang, Z. Y., Zhang, W. J., Chen, J., Liu,  
599 F. Y., Shan, X. B., and Sheng, L. S.: A Smog Chamber Facility for Qualitative and Quantitative Study on  
600 Atmospheric Chemistry and Secondary Organic Aerosol, *Chinese J Chem Phys*, 27, 631-639, 2014.
- 601 Hurley, M. D., Sokolov, O., Wallington, T. J., Takekawa, H., Karasawa, M., Klotz, B., Barnes, I., and  
602 Becker, K. H.: Organic aerosol formation during the atmospheric degradation of toluene, *Environmental*  
603 *Science & Technology*, 35, 1358-1366, 2001.
- 604 Johnson, D., Jenkin, M. E., Wirtz, K., and Martin-Reviejo, M.: Simulating the Formation of Secondary  
605 Organic Aerosol from the Photooxidation of Toluene, *Environmental Chemistry*, 1, 150-165, 2004.
- 606 Kang, E., Root, M. J., Toohey, D. W., and Brune, W. H.: Introducing the concept of Potential Aerosol  
607 Mass (PAM), *Atmospheric Chemistry And Physics*, 7, 5727-5744, 2007.
- 608 Kolev, S. and Grigorieva, V.: Surface and Total Ozone Over Bulgaria, Dordrecht, 351-358,
- 609 Lambe, A. T., Chhabra, P. S., Onasch, T. B., Brune, W. H., Hunter, J. F., Kroll, J. H., Cummings, M. J.,  
610 Brogan, J. F., Parmar, Y., Worsnop, D. R., Kolb, C. E., and Davidovits, P.: Effect of oxidant concentration,  
611 exposure time, and seed particles on secondary organic aerosol chemical composition and yield,  
612 *Atmospheric Chemistry and Physics*, 15, 3063-3075, 10.5194/acp-15-3063-2015, 2015.
- 613 Lane, D. A. and Tang, H.: Photochemical Degradation of Polycyclic Aromatic Compounds. I.  
614 Naphthalene, *Polycyclic Aromatic Compounds*, 5, 131-138, 1994.
- 615 Leone, J. A., Flagan, R. C., Grosjean, D., and Seinfeld, J. H.: An Outdoor Smog Chamber And Modeling  
616 Study Of Toluene-Nox Photooxidation, *International Journal Of Chemical Kinetics*, 17, 177-216, 1985.
- 617 Leone, J. A., Flagan, R. C., Grosjean, D., and Seinfeld, J. H.: An outdoor smog chamber and modeling



- 618 study of toluene–NO<sub>x</sub> photooxidation, *International Journal of Chemical Kinetics*, 17, 177-216, 2010.
- 619 Li, J. L., Li, H., Wang, X. Z., Wang, W. G., Ge, M. F., Zhang, H., Zhang, X., Li, K., Chen, Y., Wu, Z. H.,  
620 Chai, F. H., Meng, F., Mu, Y. J., Mellouki, A., Bi, F., Zhang, Y. J., Wu, L. Y., and Liu, Y. C.: A large-scale  
621 outdoor atmospheric simulation smog chamber for studying atmospheric photochemical processes:  
622 Characterization and preliminary application, *J Environ Sci-China*, 102, 185-197, 2021.
- 623 Li, K. W., Chen, L. H., Han, K., Lv, B. A., Bao, K. J., Wu, X. C., Gao, X., and Cen, K. F.: Smog chamber  
624 study on aging of combustion soot in isoprene/SO<sub>2</sub>/NO<sub>x</sub> system: Changes of mass, size, effective density,  
625 morphology and mixing state, *Atmospheric Research*, 184, 139-148, 2017.
- 626 Liu, S. J., Tsona, N. T., Zhang, Q., Jia, L., Xu, Y. F., and Du, L.: Influence of relative humidity on  
627 cyclohexene SOA formation from OH photooxidation, *Chemosphere*, 231, 478-486, 2019.
- 628 Liu, T., Chan, A. W. H., and Abbatt, J. P. D.: Multiphase Oxidation of Sulfur Dioxide in Aerosol Particles:  
629 Implications for Sulfate Formation in Polluted Environments, *Environ Sci Technol*, 55, 4227-4242,  
630 10.1021/acs.est.0c06496, 2021.
- 631 Liu, T. Y. and Abbatt, J. P. D.: Oxidation of sulfur dioxide by nitrogen dioxide accelerated at the interface  
632 of deliquesced aerosol particles, *Nature chemistry*, 13, 1173-1177, 10.1038/s41557-021-00777-0, 2021.
- 633 Lutz, A., Mohr, C., Le Breton, M., Lopez-Hilfiker, F. D., Priestley, M., Thornton, J. A., and Hallquist,  
634 M.: Gas to Particle Partitioning of Organic Acids in the Boreal Atmosphere, *ACS Earth and Space*  
635 *Chemistry*, 3, 1279-1287, 10.1021/acsearthspacechem.9b00041, 2019.
- 636 Ma, W., Liu, Y., Zhang, Y., Feng, Z., Zhan, J., Hua, C., Ma, L., Guo, Y., Zhang, Y., Zhou, W., Yan, C.,  
637 Chu, B., Chen, T., Ma, Q., Liu, C., Kulmala, M., Mu, Y., and He, H.: A New Type of Quartz Smog  
638 Chamber: Design and Characterization, *Environ Sci Technol*, 56, 2181-2190, 10.1021/acs.est.1c06341,  
639 2022.
- 640 Martin-Reviejo, M. and Wirtz, K.: Is benzene a precursor for secondary organic aerosol?, *Environmental*  
641 *Science & Technology*, 39, 1045-1054, 2005.
- 642 Mekic, M., Liu, J., Zhou, W., Loisel, G., and Gligorovski, S.: Formation of highly oxygenated  
643 multifunctional compounds from cross-reactions of carbonyl compounds in the atmospheric aqueous  
644 phase, *Atmospheric Environment*, 219, 117046, 2019.
- 645 Mellouki, A.: Atmospheric Fate of Unsaturated Ethers, *Dordrecht*, 163-169,
- 646 Mocanu, R., Cucu-Man, S., and Steinnes, E.: Heavy Metals Pollution: An Everlasting Problem,  
647 *Dordrecht*, 359-368,
- 648 Morriss, F. V., Bolze, C., Goodwin, J. T., and King, F.: Smog Experiments In Large Chambers, *Industrial*  
649 *And Engineering Chemistry*, 49, 1249-1250, 1957.
- 650 Odum, J. R., Hoffmann, T., Bowman, F., Collins, D., Flagan, R. C., and Seinfeld, J. H.: Gas/particle  
651 partitioning and secondary organic aerosol yields, *Environmental Science & Technology*, 30, 2580-2585,  
652 1996.
- 653 Odum, J. R., Jungkamp, T. P. W., Griffin, R. J., Forstner, H. J. L., Flagan, R. C., and Seinfeld, J. H.:  
654 Aromatics, reformulated gasoline, and atmospheric organic aerosol formation, *Environmental Science &*  
655 *Technology*, 31, 1890-1897, 1997.
- 656 Olariu, R.-I., Duncianu, M., Arsene, C., and Wirtz, K.: Determination of Photolysis Frequencies for  
657 Selected Carbonyl Compounds in the EUPHORE Chamber Environmental, *Dordrecht*, 121-128,
- 658 Pöschl, U. and Shiraiwa, M.: Multiphase chemistry at the atmosphere-biosphere interface influencing  
659 climate and public health in the anthropocene, *Chemical reviews*, 115, 4440-4475, 10.1021/cr500487s,  
660 2015.
- 661 Pandis, S. N., Paulson, S. E., Seinfeld, J. H., and Flagan, R. C.: Aerosol Formation In the Photooxidation



- 662 Of Isoprene And Beta-Pinene, *Atmos Environ a-Gen*, 25, 997-1008, 1991.
- 663 Paulsen, Dommen, Kalberer, Prevot, ASH, Richter, Sax, Steinbacher, Weingartner, and Baltensperger:  
664 Secondary organic aerosol formation by irradiation of 1,3,5-trimethylbenzene-NO<sub>x</sub>-H<sub>2</sub>O in a new  
665 reaction chamber for atmospheric chemistry and physics, *Environmental Science & Technology*, 39,  
666 2668-2678, <https://doi.org/10.1021/es0489137>, 2005.
- 667 Peng, J., Hu, M., Guo, S., Du, Z., Shang, D., Zheng, J., Zheng, J., Zeng, L., Shao, M., Wu, Y., Collins,  
668 D., and Zhang, R.: Ageing and hygroscopicity variation of black carbon particles in Beijing measured by  
669 a quasi-atmospheric aerosol evolution study (QUALITY) chamber, *Atmospheric Chemistry and Physics*,  
670 17, 10333-10348, 10.5194/acp-17-10333-2017, 2017.
- 671 Platt, S. M., El Haddad, I., Zardini, A. A., Clairrotte, M., Astorga, C., Wolf, R., Slowik, J. G., Temime-  
672 Roussel, B., Marchand, N., Jezek, I., Drinovec, L., Mocnik, G., Mohler, O., Richter, R., Barmet, P.,  
673 Bianchi, F., Baltensperger, U., and Prevot, A. S. H.: Secondary organic aerosol formation from gasoline  
674 vehicle emissions in a new mobile environmental reaction chamber, *Atmospheric Chemistry And Physics*,  
675 13, 9141-9158, 2013.
- 676 Pratap, V., Carlton, A. G., Christiansen, A. E., and Hennigan, C. J.: Partitioning of Ambient Organic  
677 Gases to Inorganic Salt Solutions: Influence of Salt Identity, Ionic Strength, and pH, *Geophysical*  
678 *Research Letters*, 48, 10.1029/2021gl095247, 2021.
- 679 Ravishankara, A. R.: Heterogeneous and multiphase chemistry in the troposphere, *Science*, 276, 1058-  
680 1065, 1997.
- 681 Reid, J. P., Bertram, A. K., Topping, D. O., Laskin, A., Martin, S. T., Petters, M. D., Pope, F. D., and  
682 Rovelli, G.: The viscosity of atmospherically relevant organic particles, *Nature communications*, 9, 956,  
683 10.1038/s41467-018-03027-z, 2018.
- 684 Ren, Y. G., Grosselin, B., Daele, V., and Mellouki, A.: Investigation of the reaction of ozone with isoprene,  
685 methacrolein and methyl vinyl ketone using the HELIOS chamber, *Faraday Discussions*, 200, 289-311,  
686 2017.
- 687 Rollins, A. W., Kiendler-Scharr, A., Fry, J. L., Brauers, T., Brown, S. S., Dorn, H. P., Dube, W. P., Fuchs,  
688 H., Mensah, A., Mentel, T. F., Rohrer, F., Tillmann, R., Wegener, R., Wooldridge, P. J., and Cohen, R. C.:  
689 Isoprene oxidation by nitrate radical: alkyl nitrate and secondary organic aerosol yields, *Atmospheric*  
690 *Chemistry And Physics*, 9, 6685-6703, 2009.
- 691 Rudzinski, K. J.: Heterogeneous and Aqueous-Phase Transformations of Isoprene, Dordrecht, 261-277,  
692 Stern, J. E., Flagan, R. C., Grosjean, D., and Seinfeld, J. H.: Aerosol Formation And Growth In  
693 Atmospheric Aromatic Hydrocarbon Photooxidation, *Environmental Science & Technology*, 21, 1224-  
694 1231, 1987.
- 695 Su, H., Cheng, Y., and Poschl, U.: New Multiphase Chemical Processes Influencing Atmospheric  
696 Aerosols, Air Quality, and Climate in the Anthropocene, *Accounts of chemical research*, 53, 2034-2043,  
697 10.1021/acs.accounts.0c00246, 2020.
- 698 Su, H., Cheng, Y., Zheng, G., Wei, C., Mu, Q., Zheng, B., Wang, Z., Zhang, Q., He, K., and Carmichael,  
699 G.: Reactive nitrogen chemistry in aerosol water as a source of sulfate during haze events in China,  
700 *Science Advances*, 2, e1601530-e1601530, 2016.
- 701 Takekawa, H., Minoura, H., and Yamazaki, S.: Temperature dependence of secondary organic aerosol  
702 formation by photo-oxidation of hydrocarbons, *Atmospheric Environment*, 37, 3413-3424, 2003.
- 703 Thuner, L. P., Bardini, P., Rea, G. J., and Wenger, J. C.: Kinetics of the gas-phase reactions of OH and  
704 NO<sub>3</sub> radicals with dimethylphenols, *Journal Of Physical Chemistry A*, 108, 11019-11025, 2004.
- 705 Tolkacheva, G. A.: Problems of Air Quality in Tashkent City, Dordrecht, 379-392,



- 706 Turšič, J., Grgić, I., and Podkrajšek, B.: Influence of ionic strength on aqueous oxidation of SO<sub>2</sub>  
707 catalyzed by manganese, *Atmospheric Environment*, 37, 2589-2595, 10.1016/s1352-2310(03)00215-2,  
708 2003.
- 709 Virtanen, A., Joutsensaari, J., Koop, T., Kannosto, J., Yli-Pirila, P., Leskinen, J., Makela, J. M.,  
710 Holopainen, J. K., Poschl, U., Kulmala, M., Worsnop, D. R., and Laaksonen, A.: An amorphous solid  
711 state of biogenic secondary organic aerosol particles, *Nature*, 467, 824-827, 10.1038/nature09455, 2010.
- 712 Wang, B., O'Brien, R. E., Kelly, S. T., Shilling, J. E., Moffet, R. C., Gilles, M. K., and Laskin, A.:  
713 Reactivity of liquid and semisolid secondary organic carbon with chloride and nitrate in atmospheric  
714 aerosols, *The journal of physical chemistry. A*, 119, 4498-4508, 10.1021/jp510336q, 2015a.
- 715 Wang, G. H., Zhang, R. Y., Gomez, M. E., Yang, L. X., Zamora, M. L., Hu, M., Lin, Y., Peng, J. F., Guo,  
716 S., Meng, J. J., Li, J. J., Cheng, C. L., Hu, T. F., Ren, Y. Q., Wang, Y. S., Gao, J., Cao, J. J., An, Z. S.,  
717 Zhou, W. J., Li, G. H., Wang, J. Y., Tian, P. F., Marrero-Ortiz, W., Secret, J., Du, Z. F., Zheng, J., Shang,  
718 D. J., Zeng, L. M., Shao, M., Wang, W. G., Huang, Y., Wang, Y., Zhu, Y. J., Li, Y. X., Hu, J. X., Pan, B.,  
719 Cai, L., Cheng, Y. T., Ji, Y. M., Zhang, F., Rosenfeld, D., Liss, P. S., Duce, R. A., Kolb, C. E., and Molina,  
720 M. J.: Persistent sulfate formation from London Fog to Chinese haze, *Proceedings Of the National  
721 Academy Of Sciences Of the United States Of America*, 113, 13630-13635, 10.1073/pnas.1616540113,  
722 2016.
- 723 Wang, J., Doussin, J. F., Perrier, S., Perraudin, E., Katrib, Y., Pangu, E., and Picquet-Varrault, B.: Design  
724 of a new multi-phase experimental simulation chamber for atmospheric photo-smog, aerosol and cloud  
725 chemistry research, *Atmospheric Measurement Techniques*, 4, 2465-2494, 2011.
- 726 Wang, W. G., Li, K., Zhou, L., Ge, M. F., Hou, S. Q., Tong, S. R., Mu, Y. J., and Jia, L.: Evaluation and  
727 Application of Dual-Reactor Chamber for Studying Atmospheric Oxidation Processes and Mechanisms,  
728 *Acta Physico-Chimica Sinica*, 31, 1251-1259, 2015b.
- 729 Wang, X., Liu, T., Bernard, F., Ding, X., Wen, S., Zhang, Y., Zhang, Z., He, Q., Lü, S., Chen, J., Saunders,  
730 S., and Yu, J.: Design and characterization of a smog chamber for studying gas-phase chemical  
731 mechanisms and aerosol formation, *Atmospheric Measurement Techniques*, 7, 301-313, 10.5194/amt-7-  
732 301-2014, 2014.
- 733 Warneke and C.: Comparison of daytime and nighttime oxidation of biogenic and anthropogenic VOCs  
734 along the New England coast in summer during New England Air Quality Study 2002, *Journal of  
735 Geophysical Research Atmospheres*, 109, D10309, 2004.
- 736 Wenger, J. C.: *Chamber Studies on the Photolysis of Aldehydes* Environmental, Dordrecht, 111-119,
- 737 White, S., Angove, D., Li, K. W., Campbell, I., Element, A., Halliburton, B., Lavrencic, S., Cameron, D.,  
738 Jamie, I., and Azzi, M.: Development of a new smog chamber for studying the impact of different UV  
739 lamps on SAPRC chemical mechanism predictions and aerosol formation, *Environmental Chemistry*, 15,  
740 171-182, 2018.
- 741 Wu, S., Lu, Z. F., Hao, J. M., Zhao, Z., Li, J. H., Hideto, T., Hiroaki, M., and Akio, Y.: Construction and  
742 characterization of an atmospheric simulation smog chamber, *Adv Atmos Sci*, 24, 250-258, 2007.
- 743 Zhang, Y., Sanchez, M. S., Douet, C., Wang, Y., Bateman, A. P., Gong, Z., Kuwata, M., Renbaum-Wolff,  
744 L., Sato, B. B., Liu, P. F., Bertram, A. K., Geiger, F. M., and Martin, S. T.: Changing shapes and implied  
745 viscosities of suspended submicron particles, *Atmospheric Chemistry And Physics*, 15, 7819-7829, 2015.
- 746 Zhang, Y., Chen, Y., Lei, Z., Olson, N. E., Riva, M., Koss, A. R., Zhang, Z., Gold, A., Jayne, J. T.,  
747 Worsnop, D. R., Onasch, T. B., Kroll, J. H., Turpin, B. J., Ault, A. P., and Surratt, J. D.: Joint Impacts of  
748 Acidity and Viscosity on the Formation of Secondary Organic Aerosol from Isoprene Epoxydiols  
749 (IEPOX) in Phase Separated Particles, *ACS Earth and Space Chemistry*, 3, 2646-2658,





750 10.1021/acsearthspacechem.9b00209, 2019.  
751 Zhang, Y., Chen, Y., Lambe, A. T., Olson, N. E., Lei, Z., Craig, R. L., Zhang, Z., Gold, A., Onasch, T. B.,  
752 Jayne, J. T., Worsnop, D. R., Gaston, C. J., Thornton, J. A., Vizuete, W., Ault, A. P., and Surratt, J. D.:  
753 Effect of the Aerosol-Phase State on Secondary Organic Aerosol Formation from the Reactive Uptake of  
754 Isoprene-Derived Epoxydiols (IEPOX), *Environmental Science & Technology Letters*, 5, 167-174,  
755 10.1021/acs.estlett.8b00044, 2018.  
756 Zheng, J., Shi, X. W., Ma, Y., Ren, X. R., Jabbour, H., Diao, Y. W., Wang, W. W., Ge, Y. F., Zhang, Y. C.,  
757 and Zhu, W. H.: Contribution of nitrous acid to the atmospheric oxidation capacity in an industrial zone  
758 in the Yangtze River Delta region of China, *Atmospheric Chemistry And Physics*, 20, 5457-5475, 2020.  
759 Zhou, S., Hwang, B. C. H., Lakey, P. S. J., Zuend, A., Abbatt, J. P. D., and Shiraiwa, M.: Multiphase  
760 reactivity of polycyclic aromatic hydrocarbons is driven by phase separation and diffusion limitations,  
761 *Proc Natl Acad Sci U S A*, 116, 11658-11663, 10.1073/pnas.1902517116, 2019.  
762 Zielinska, B., Sagebiel, J., Stockwell, W., McDonald, J., Seagrave, J., Wiesen, P., and Wirtz, K.:  
763 Investigation of Atmospheric Transformations of Diesel Emissions in the European Photoreactor  
764 (EUPHORE), Dordrecht, 279-284,  
765 Ziemann, P. J. and Atkinson, R.: Kinetics, products, and mechanisms of secondary organic aerosol  
766 formation, *Chemical Society reviews*, 41, 6582-6605, 10.1039/c2cs35122f, 2012.  
767